

SYSTEM DESIGN FOR SELF-SEEDING THE LCLS AT SOFT X-RAY ENERGIES*

Y. Feng[#], J. Amann, D. Cocco, C. Field, J. Hastings, P. Heimann, Z. Huang, H. Loos, J. Welch, J. Wu, SLAC, Menlo Park CA 94025, U.S.A.

K. Chow, P. Emma, N. Rodes, R. Schoenlein, LBNL, Berkeley, CA 94720, U.S.A.

Abstract

The complete design for self-seeding the LCLS at soft X-ray energies from 500 to 1000 eV based on a grating monochromator is described. The X-ray optics system consists of a toroidal variable-line-space (VLS) grating and focusing mirrors for imaging the seed pulse onto the downstream seeding undulator. The system has a resolving power greater than 5000 creating a near-transform-limited seed pulse from the upstream SASE undulator for pulse durations up to 36 fs FWHM at 500 eV and 18 fs FWHM at 1000 eV. Diagnostics for ensuring overlap with the electron beam are included in the design. The optical system is sufficiently compact to fit within a single 3.9 m LCLS undulator segment. The electron chicane system which serves to delay the electron beam to match the less than 1 ps delay from the optical system is similar to the chicane used in the hard X-ray self-seeding at LCLS. The seeded FEL pulse is expected to be nearly transform-limited with a bandwidth in the 2×10^{-4} range, potentially increasing the low-charge FEL X-ray peak spectral brightness by 1 to 2 orders of magnitude.

INTRODUCTION

LCLS presently produces X-ray radiation that is transversely coherent but not longitudinally. The temporal profile is a spiky structure characteristic of the SASE process that starts from the shot noise in the electron beam. The spectral domain has a similar spiky profile [1] and has been observed experimentally for soft [2] and hard [3] X-rays. Seeding (overlapping) the electron beam with a monochromatic X-ray beam of sufficiently narrow bandwidth and sufficient power would force the FEL to produce nearly transform-limited pulses, minimal jitter in X-ray wavelength and potentially higher spectral brightness by 1 to 2 orders of magnitude if taken to full saturation. These enhanced beam qualities will benefit the users by not only improving the measurement efficiency and data analysis, but also enabling experimental studies in many areas of biology, materials, chemistry, and atomic, molecular, and optical sciences where high spectral brightness or high peak power is essential.

* Portions of this research were carried out at the Linac Coherent Light Source (LCLS) at the SLAC National Accelerator Laboratory. LCLS is an Office of Science User Facility operated for the U.S. Department of Energy Office of Science by Stanford University under Contract No. DE-AC02-76SF00515. LBNL part of work is supported by the Director, Office of Science, of the U.S. Department of Energy under Contract No. DE-AC02-05CH11231
#yfeng@slac.stanford.edu

A possible concept for self-seeding, originally proposed by a DESY team [4], uses a grating monochromator between a SASE and seeding undulator to generate the soft X-ray seed. This principle was adopted for a conceptual design aimed at seeding the future LCLS-II soft X-ray undulator between 200 and 2000 eV with a minimum bandwidth of 5×10^{-5} [5]. A more compact X-ray optics design ensued for the current LCLS soft X-ray undulator in a limited energy range with a more modest bandwidth requirement of 2×10^{-4} [6]. Following the successful demonstration of the hard X-ray self-seeding (HXRSS) at LCLS using a thin diamond monochromator in transmission [7], there is a pressing need for a parallel implementation in the soft X-ray energies. To preserve the performance of the current LCLS FEL, it is necessary that the X-ray optics be designed such that the entire seeding system fit within a single 3.4 m LCLS undulator segment space in an arrangement similar to that of the HXRSS. This paper describes the overall design of the system for soft X-ray self-seeding (SXRSS) the LCLS.

SEEDING SYSTEM OVERVIEW

The SXRSS system, proposed to replace the existing U9 undulator segment, is shown schematically Figure 1. It consists of 3 major components: 1) a complete grating monochromator system with its vacuum vessel and internal motions, isolation valves, pumps, and gauges, and all necessary mechanical supports to the existing undulator girder; 2) A weak four-dipole magnetic chicane, five rack-mountable power supplies (1 main & 4 trims) and appropriate cables, chicane vacuum chamber, and all necessary mechanical supports to the existing U9 sliders; 3) Diagnostics to measure the overlap of the electron and seeding X-ray beams.

The system supports both the seeded and SASE mode. In the seeded mode, the magnetic chicane is powered, and the electron beam breaks from co-propagation with X-rays in the upstream SASE undulator U8 at the first dipole B1 of the chicane and is displaced with proper delay and then re-introduced into the downstream seeding undulator U10 after the fourth dipole B4. The SASE X-rays are monochromatized by the grating, the mirror M1 and the slit and imaged by the mirrors M2 and M3 onto the mid-section of the immediate downstream undulator U10 to merge with the electron beam to seed the FEL process. X-ray and electron diagnostics (not shown) are distributed strategically to ensure spatial and pointing overlap of the two beams.

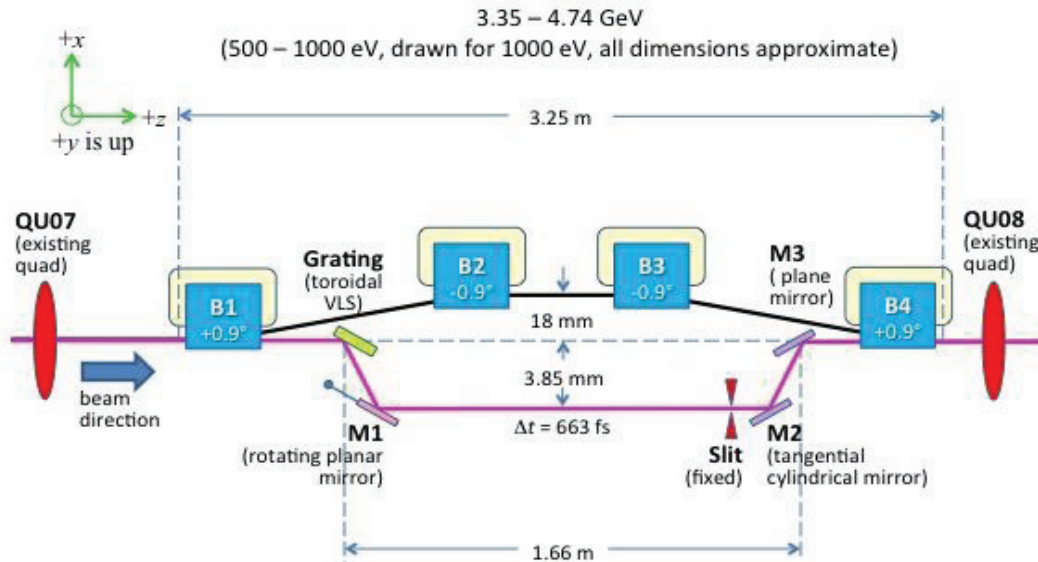


Figure 1: Layout of the LCLS compact SXRSS system to be located in the space vacated by undulator U9. The grating is a toroidal VLS type, M1 is a rotating plane mirror, M2 a tangential cylindrical mirror, and M3 a plane mirror used to steer the beam. The system is drawn for the 1000 eV settings (663 fs delay) with all dimensions approximate. The deflections of the electron and photon beams are both in the horizontal plane only.

Table 1: LCLS SXRSS Performance Specifications

Parameter	Nominal	Min	Max	Unit
Photon energy	500-1000	300	1200	eV
Electron energy	3.35-4.74	2.6	5.2	GeV
Repetition rate	120	1	120	Hz
Bunch charge	150	10	250	pC
e- bunch length (FWHM)	50	5	100	fs
γ bunch length (FWHM)	36-18	-	-	fs
Photon bandwidth	2×10^{-4}	-	-	-

For operation in SASE mode when seeding is not desired, the magnetic chicane is de-powered, and the entire grating system retracted allowing the electron and X-rays continue co-propagation through the entire section nearly unperturbed. Switching between SASE and seeded modes should be possible in a few minutes. The overall SXRSS performance specifications for seeding are listed in Table 1. The nominal range of photon energy refers to the energies for which good resolving power and thus narrow bandwidth can be achieved. The minimum and maximum values are accessible with the machine parameters, but the seeding performance may be degraded considerably.

GRATING MONOCHROMATOR

The SXRSS grating monochromator system was designed with refinement from previous concepts to meet the overall physics requirements:

- To fit within a single LCLS undulator section of 3.87 m.

- A resolving power greater than or equal to 5000 to produce a nearly transform-limited seed X-ray pulse.
- Photon operating energy range from 500 to 1000 eV.
- An optical delay less than 1 ps. A variable delay is acceptable.
- To generate 20 kW seed power, sufficient for producing seeding with optimal spectral properties.
- To produce a nearly 1:1 image of the X-ray beam at the source point in the SASE undulator onto the re-entrant point in the seeding undulator.
- To maintain a stay-clear distance of 2.5 mm between the electron beam and including all optics and mechanical components.
- To provide beam steering capability to ensure maximum overlap between the X-ray and electron beams.

The complete X-ray monochromator system is shown in Figure 1. The optical system consists of a toroidal variable-line-spacing [8] (VLS) grating that disperses the X-rays, a plane mirror M1, an exit slit, a tangentially cylindrical focusing mirror M2, and a plane mirror M3 for directing the X-ray beam onto the electron beam. The grating, with the tangential curvature in conjunction with the VLS construction, focuses at the slit. The grating sagittal curvature images at the re-entrant point in the mid-section of the seeding undulator U10. The horizontally divergent beam emerging from the slit is re-focused by M2 onto the re-entrant point as well, completing a nearly 1:1 imaging of the source point in both transverse directions. The post-mirror M1 re-directs the dispersed X-rays onto the fixed exit slit. M1, the exit slit, and M2 are collinear and the principal ray joining them is parallel to the original X-ray beam direction. No entrance slit is required in the FEL case since the source works effectively as that.

Toroidal VLS Grating

Since the LCLS FEL X-ray beam is highly collimated (angular divergence $\approx 20 \mu\text{rad}$ at 1000 eV), achieving the desired resolving power requires focusing of the dispersed radiation to create spatial separation of energies. The choice was made to use a variable-line-spacing grating where the line density varies in the direction perpendicular to the grooves as in the original compact design [6]. However, after taking into account the fact that the source point in the SASE undulator moves upstream with increasing X-ray energy by as much as 1.2 m over the photon energy range of 500 to 1000 eV [9], the “fixed-focus mode” previously imposed on the grating design [6] became less effective in keeping a constant focus. As such a tangential radius was introduced in the grating to minimize the variation in the image distance as a function of energy while keeping the incidence angle constant using the grating focusing equation $F_{20} = -n\lambda D_1 + (\cos^2 \alpha r + \cos^2 \beta r' - \cos \alpha R - \cos \beta R)$, where $n=1$, λ , D_1 , α , β are the diffraction order, X-ray wavelength, the 1st order coefficient of VLS, incident and diffraction angles, R the tangential radius, r and r' the source and image distances. The object distance was based on FEL simulation of the LCLS undulator at the exit of U9 [9].

Table 2: Grating and Slit Parameters

Parameter	Value	Required Precision	Unit
Line density (D_0)	1123	0.2%	1/mm
Linear coeff. (D_1)	1.6	1%	1/mm ²
Quad. coeff. (D_2)	0.002	100%	1/mm ³
Groove profile	blazed 1.2°	-	n/a
Tangential radius	195	1%	m
Sagittal radius	18	5%	cm
Diffraction order	+1	-	-
Incident angle	89.00	-	°
Exit angle	85.61-86.82	-	°
Source distance	2972-4157	-	mm
Source size	30.6-24.7	-	μm
Image distance	1346.7-1348	-	mm
Image size	3-2.4	-	μm
Exit slit location	1350	1	mm
Exit slit size	variable	-	μm
Optical delay	797.9-662.8	-	fs

The sagittal radius of curvature was also introduced into the grating to provide focusing in the direction normal to the dispersion plane. Without focusing, the beam size could grow 6 fold at 500 eV at the re-entrant point to over 160 μm , reducing the seeding power

significantly. The fixed incident angle produced a fixed focal length, minimizing the change in the location of the focus in the sagittal plane. The complete list of parameters for this toroidal grating is given in Table 2.

Focusing at Slit

The waist size of the focus near the slit was found to vary nearly linearly from 3 μm at 500 eV to 2.4 μm at 1000 eV. Both ray-optics and Gaussian beam calculations were made. The small difference is a result of the fact that the source distance is well into the far-field zone due to the small source, and thus short Rayleigh range. The location of the focus was found to vary by ~ 2 mm in the design energy range from 500 to 1000 eV around the slit due to the variation in source point location. As such, the wavefront at the slit is not strictly flat, and the virtual source point created by the slit is no longer at the slit as in the case for incoherent X-ray radiation. This defocusing effect was fully accounted for in the Gaussian optics treatment by retaining the wavefront curvature in propagation to the downstream optical components.

Energy Tuning

The grating will operate in the so-called “fixed incidence angle mode” in the +1 order. X-ray energy tuning is achieved by a single rotation of M1. This tuning operation is simpler than the previous design [6] where both the grating and the mirror are required to rotate in concerted motions. In the current operating mode, there are still variations in the total optical path, resulting in an energy dependent delay from 798 fs at 500 eV to 663 fs at 1000 eV as indicated in Table 1. The total tuning from 500 to 1000 eV requires a change in the M1 mirror angle by approximately 10 mrad in total.

Resolving Power

Resolving power is achieved by the combination of the grating and the exit slit, and the estimated values are shown in Figure 2. The design goal of 5000 over the full energy range is achieved and produces near-transform-limited seed pulses for durations up to 36 fs (FWHM) at 500 eV and 18 fs (FWHM) at 1000 eV. The estimate includes contributions from the number of illuminated grooves, the size of the FEL source, the size of the exit slit in the dispersion plane at 3 μm , a slope error of 0.25 μrad for the grating and M1 mirror. The performance was calculated using the ABCD matrix method [10] applied to fully coherent Gaussian beams [11] and for VLS gratings [8]. All contributions are of the same order of magnitude, so care must be taken to ensure the assumed specifications are met in the actual construction of the system. The exact location of the focus was found to vary with energy around the slit by ~ 2 mm, which is small compared to the Rayleigh range of ~ 8 mm calculated for the focal size of 3 μm FWHM at 500 eV. As such, the impact of this de-focusing effect on the resolving power is negligible. Due to the relatively small source size, the current optics design is mostly in the far-field, and ray-optics and ray-tracing calculations yielded very similar

results to those obtained using the full coherent Gaussian beam treatment.

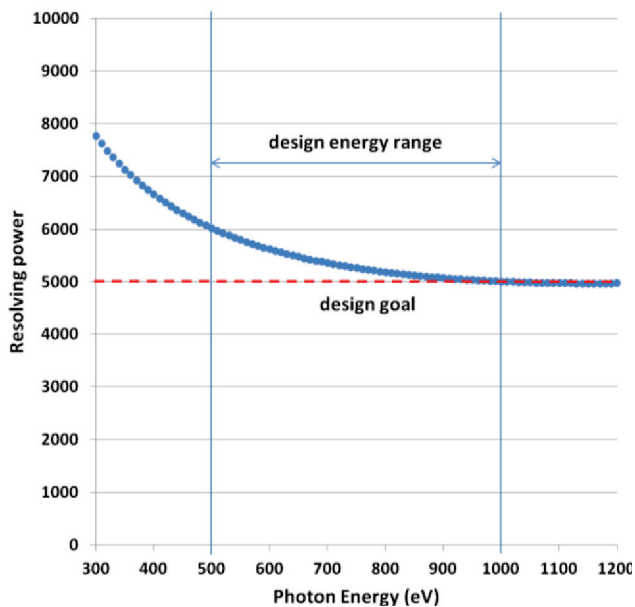


Figure 2: Calculated resolving power of the grating, including contribution from the number of illuminated grooves, source size, slope error at $0.25 \mu\text{rad}$, and a constant exit slit size of $3 \mu\text{m}$.

Groove Profile and Grating Efficiency

Due to damage concerns, the efficiency of the grating bears important discussions. With everything being equal, a lower efficiency system would require a higher input power on the grating to generate a sufficiently strong seed, thus creating a potentially damage condition to the grating and the associated optics. Using a laminar grating rather than a blazed grating has the advantage of better harmonic contamination reduction. On the other hand, a blazed grating has higher diffraction efficiency and offers the very important advantage for FEL applications that it can sustain higher peak power pulses. For laminar gratings a fraction of the radiation is absorbed at near-normal incidence on the leading edge of the lands. This condition does not exist for blazed gratings. Since tolerances on the grating to achieve the target resolution are relatively relaxed and the harmonic contribution is not an issue for the present design. This leads to the clear choice of a blazed grating for our application. The efficiency of the grating depends on the blaze angle. For the specified operating range, 500-1000 eV, the best blaze angle is 1.2° and the expected grating efficiency with a platinum coating is shown in Figure 3. The peak dose in platinum coating was estimated to be 0.05 eV/atom , about a factor of 10 below the melting threshold, and thus was deemed safe.

Pulse-front Tilt and Elongation

As with any dispersive optical element, the grating produces a one-dimensional pulse-front tilt by virtue of the exit angle not being identical to the incident angle and

the principal rays striking the neighbouring grooves will differ in optical path by exactly one wavelength required by the grating equation. Consequently, the pulse is elongated temporally as well when projected longitudinally. From simple geometry, the tilt angle A and elongation ΔT are given by $A = \tan^{-1}(R\lambda/w)$ and $\Delta T = R\lambda/c$, respectively, where R , λ , and w are the resolving power, X-ray wavelength, and the FWHM beam width in the dispersion plane. The tilt angle A varies from 22.1° at 500 eV to 14.1° at 1000 eV for an originally flat-top beam profile. The total elongation of the temporal profile ΔT varies from 50 fs at 500 eV to 21 fs at 1000 eV when calculated with the nominal resolving power of 5000. The tilt for a small beam cross-section as is the case at the slit can be rather significant. However, it can be much reduced after the beam is re-collimated by the M2 mirror at the re-entrant point in the seeding undulator where the effect of the tilt on the seeding efficiency was found to be of the order of 10 to 20 %.

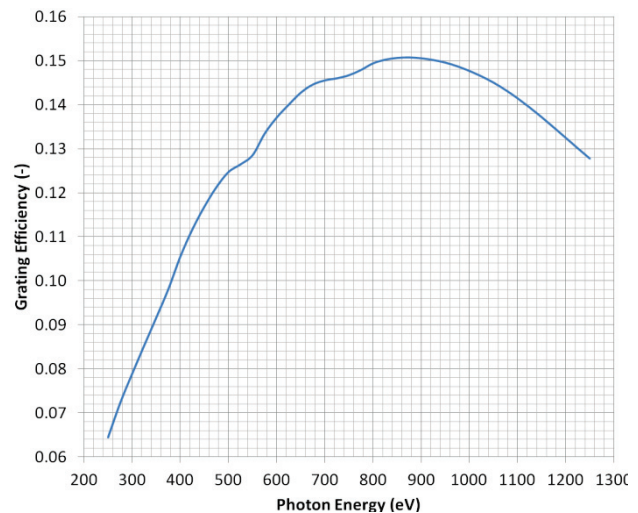


Figure 3: Calculated grating efficiency using a blazed groove profile with a blaze angle at 1.2° and platinum coating.

Imaging of Source onto Re-entrant Point

In the dispersion plane, the incident X-ray beam is imaged at the exit slit for achieving resolving power and re-imaged at the re-entrant point inside the seeding undulator for achieving the optimal overlap with the debunched electron beam. The first stage focusing is done by the VLS construction and the tangential curvature of the toroidal grating. By properly choosing the linear coefficient D_1 and the tangential radius of curvature, the focal point was nearly constant in the designed energy range. The second stage focusing is produced by a tangential cylinder mirror, M2, situated at 180 mm from the slit. With a tangential radius of curvature of 23.2 m at a constant 15 mrad incident angle. With the help of a plane mirror M3 also at a constant 15 mrad incident angle; M2 re-collimates the virtual image created by the slit onto the mid-section of the seeding undulator, U10,

for optimal spatial overlapping with the properly delayed electron beam.

In the sagittal plane, the source is imaged in a single step at the re-entrance point by the grating with the sagittal curvature. The sagittal radius of curvature is 188 mm, which at 89° incidence angle produces a variable focal length of 2.465 m at 1000 eV or 1.914 m at 500 eV. Due to the fact the source point was found by FEL simulation to vary with energy, the location of the beam waist in both dispersion and sagittal planes moved around the designated re-entrant point (mid-section of the seeding undulator U10) by as much as 2 m. As such the beam sizes in the two planes were found to be about 25% to 100% larger than at the source. Although the size mismatch relaxes the tolerance on electron and X-beam overlap, it reduces the effective seeding power. This effect was included in calculating the required SASE power for generating sufficient seed power of 20 kW.

SASE and Seed Power

According to the FEL simulation, a minimum of 20 kW for a 50 fs FWHM pulse duration is required to seed the FEL process. The overall throughput of the X-ray optics was calculated and amounted to between 4 to 7%, by including the grating efficiency, the reflectivity of all three mirrors (M1, M2 and M3), and the bandwidths mismatch between the SASE at 0.3 to 1% and the grating resolution at 0.02%. The pulse elongation and the size mismatch in both dispersion and sagittal directions reduce the effective seeding power by as much as a factor 6. The minimum SASE power was then estimated to be between 3 and 6 μ J for a 0.3% SASE bandwidth. The selection of U9 as the location of the SXRSS system should ensure sufficient SASE power incident onto the grating monochromator.

FOUR-DIPOLE CHICANE SYSTEM

The SXRSS apparatus contains four dipole magnets arranged to create a chicane in the path of the electron beam. This chicane has four functions:

- It creates a local horizontal electron trajectory offset so the electron beam avoids getting too close to the grating and mirrors.
- It washes out the SASE micro-bunching produced in the upstream undulator sections.
- It acts as an adjustable delay line for the electron bunch to match the seed x-ray delay.
- It acts as an adjustable delay line for correcting the phase error introduced by removing one undulator segment.

The chicane design was optimized so that there is at least 2 mm of clearance between the electron beam and the nearest optical element for the minimum delay setting. Generally the path length must be increased for lower photon energy (longer wavelength). X-rays of 500 eV require a maximum electron beam displacement of 17.8 mm. For the extreme case of 300 eV photons, the maximum displacement of the electron beam is 19.2 mm. In comparison, the optical delay for the hard X-ray self-

seeding [7] was much smaller by a factor at least 10, and the electron beam displacement was much smaller than that in the current chicane design.

Normal values and limiting values of electron beam chicane parameters are listed in **Table 3** along with various tolerances. In the table “Normal” refers to the performance for required photon energy range of 500 – 1000 eV (see Table 1), while “Minimum” and “Maximum” refer to the limiting values. For example, the electron beam delay varies from 930 fs at 300 eV, to 633 fs at 1200 eV, but the dipoles and vacuum chamber are capable of creating a delay of up to 1000 fs.

Table 3: Main Parameters of the Electron Beam Chicane

Parameter	Nominal	Minimum	Maximum	Unit
e- beam delay	633-930	300	1000	fs
Delay precision	0.1	0	1	fs
R ₅₆	477-397	0	600	μ m
Dipole bend angle	14.91-13.59	0	16.739	mrad
e- beam displ.	19.2-15.9	0	20	mm
H. separation	4.3-3.4	2	-	mm
Residual angle	0	0.0	0.1	μ rad
Residual offset	0	0.0	3.0	μ m

The chicane, when powered, should deflect the electrons horizontally toward the “aisle” of the undulator tunnel. Optics can only be inserted when the chicane is powered sufficiently that there is at least 2 mm of separation between the electron beam path and the nearest optical component. When not in self-seeded mode, (*i.e.*, chicane switched off), the LCLS FEL should work in the normal SASE mode except for the missing undulator and its associated phase shift. This phase shift is corrected by powering trim windings on each of the dipoles. The strength of the trim coils must be sufficient to correct the phase shift error even when running SASE beams with the highest LCLS photon energy. For 10 keV X-rays, the trim coils should be sufficient to add or subtract up to 8700 degrees of phase shift.

For seeded operation micro-bunching developed in the beam before the chicane must be suppressed to maximize the ratio of the seeded X-ray beam intensity to the SASE noise. This is accomplished through the natural energy spread of the electrons, together with the R₅₆ of the chicane.

OVERLAP DIAGNOSTICS

Efficient operation of the self-seeding system requires the electron and X-ray seed beam to overlap in the downstream undulators for about one gain length and within a fraction of the 25 μ m beam size. For the initial commissioning diagnostics to measure a 10 μ m overlap, it is sufficient to generate a seeded FEL signal which can then be used for further optimization. The diagnostics

foreseen in the long breaks downstream of undulators U9 and U12 contain a 100 μm thick YAG:Ce screen viewed with a CCD to measure the X-ray seed beam position. Radiation protection for the undulators does not allow use of the YAG:Ce crystal to diagnose the electron beam. Instead two crossed carbon wires overlaid on a central few mm diameter hole on the YAG:Ce crystal will both enable the electron beam to pass through the crystal and to provide a beam loss signal from the electron beam intercepting the wires. The electron beam position will be obtained by moving the entire diagnostic system by means of the supporting undulator girder cams similar to the LCLS undulator beam finder wire system. The relative position of the two beams can be inferred from the CCD image showing both the seed beam position on the YAG:Ce and the wires.

FEL SIMULATIONS

A start-to-end simulation was carried out to study the performance of the system at 1 keV. Simulation codes IMPACT-T and Elegant were used for the electron dynamics in the LCLS-I injector and LINAC. To match to the resolving power, a 150 pC bunch charge was used. The electron bunch longitudinal phase space is shown in Figure 4. The electron bunch is compressed to have a peak current of 3 kA in the central part, and the double-horn profile is seen as in Figure 5. The LINAC RF system is tuned so that the leading horn (on the left) is much smaller to minimize the wakefield effect in the undulator system.

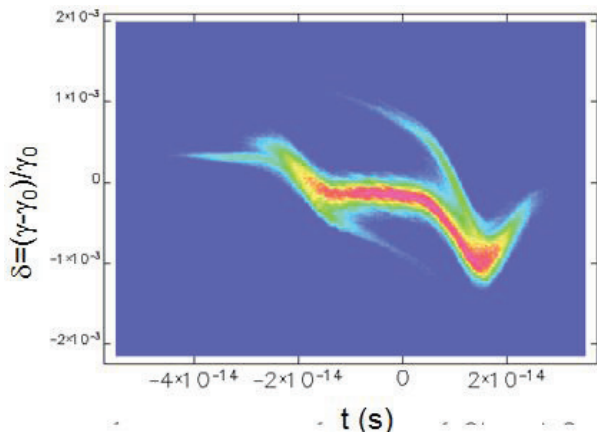


Figure 4: Longitudinal phase space of the electron bunch at the entrance of undulator system.

The electron bunch was then sent into the SASE undulator sections from U1 to U8 to simulate the SASE FEL process. The gain curve is shown in Figure 6. The vertical dash line indicates the end of U8 where enough SASE power has built up to prepare for a seed for the seeding part of the undulator system starting after the optics and the chicane at U10. In fact, according to the simulation, even at U6 (the dashed circle), there is sufficient SASE power to prepare for a seed. The FEL spectrum is shown in Figure 7 for the radiation at the 40 m mark well into saturation, exhibiting a FWHM

bandwidth of 5.7×10^{-3} with the predicated spiky features characteristics of the stochastic nature of SASE process. The spectrum at the end of U8 before the grating is very similar to that at 21 m with only slightly narrower bandwidth due to the fact that this location is still in the exponential growth regime before saturation.

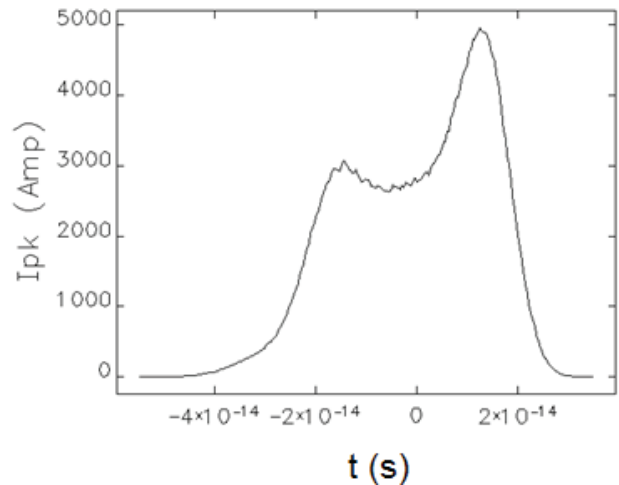


Figure 5: Double-horn profile of a 150 pC electron bunch compressed to 3 kA peak current in the central part.

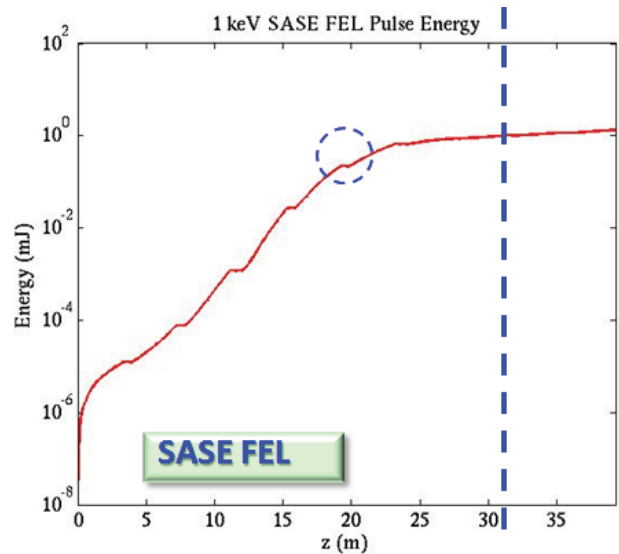


Figure 6: SASE FEL gain curve. The dashed vertical line indicates the end of U8, the dashed circle gives the operational point where there will still be sufficient input SASE power should it becomes necessary.

The broadband SASE light is then monochromatized by the grating system and recombined with the de-bunched and properly delayed electron beam to continue the seeded FEL lasing process starting at U10. The required seed power is about 20 kW, and the seeded FEL gain curve is shown in Figure 8, where the SXRSS system is the starting point at 0 m. The vertical dashed line indicates the end of U15, just before the hard x-ray self-seeding (HXRSS) monochromator and chicane section

[7]. As such the SXRSS system can reach saturation before reaching the HXRSS system should the break in the FEL amplification process created by U15 become a concern in understanding the performance of the SXRSS process.

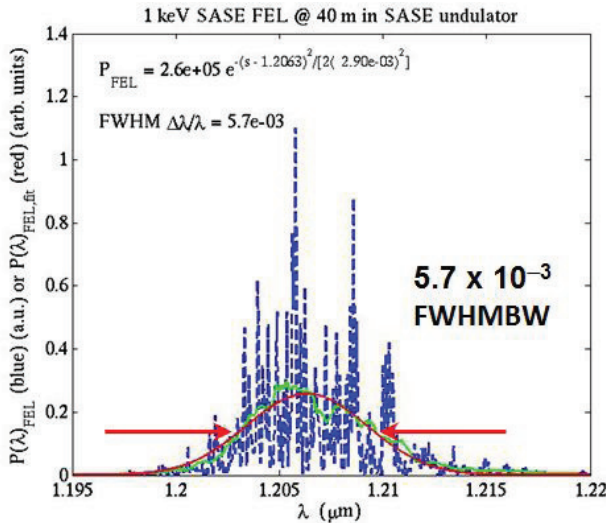


Figure 7: The spectrum of the SASE FEL spectrum at 40 m undulator, which is similar to that at the end of U8.

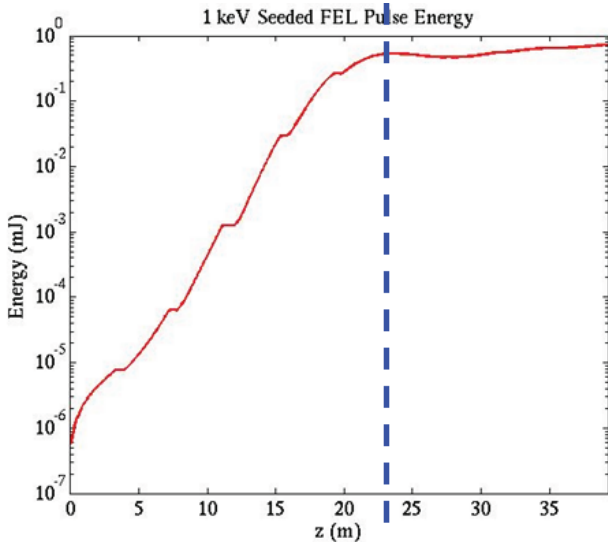


Figure 8: Seeded FEL gain curve after the SXR system at U9. The dashed vertical line indicates the end of U15.

The seeded FEL spectrum at 21 m, which is slightly before the end of U15 in the seeding undulator section, is shown in Figure 9. The FWHM bandwidth is fitted to be 1.6×10^{-4} , about 35 times narrower than that of the SASE without seeding. Given the FEL pulse duration at 50 fs (the middle flat part between the horns is slightly shorter as depicted in Figure 5), the bandwidth is close to transform limited and matched to the designed optical resolving power specification at 5000. There is still residual background close and around the seeding

wavelength, which in principle could be cleaned up by a monochromator for a cleaner experimental measurement.

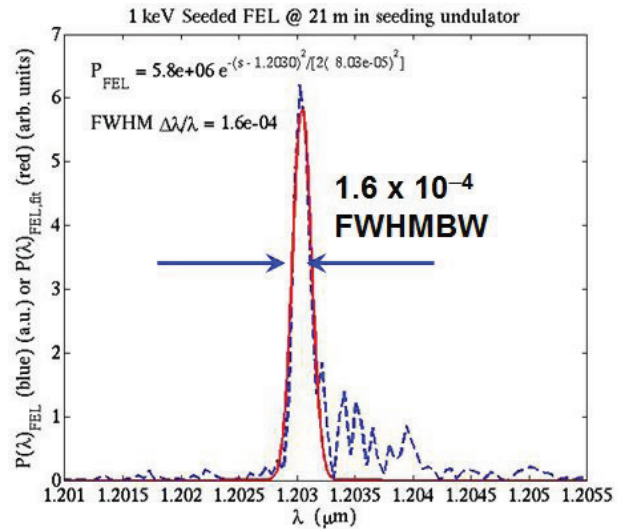


Figure 9: The spectrum of the seeded FEL spectrum at 21 m mark in the seeding undulator after the SXRSS section at 0 m.

In summary, the strong scientific case requiring higher spectral brightness has clearly been made. For LCLS as a user facility, a self-seeding scheme provides the best choice in not requiring significant changes to the LCLS-I undulator structure and allowing an immediate implementation. The system design for the LCLS SXRSS is near completion including the X-ray optics, the chicane, the overlap diagnostics and the mechanical components. FEL simulation supports soft X-ray seeding at LCLS with optimal spectral performance producing nearly transform-limited pulses with greater than 30 times increased spectral brightness.

ACKNOWLEDGMENT

Y. Feng wishes to thank M. Rowen and J. Krzywinski for their expertises and help in the earlier stage of the SXRSS concept design. Portions of this research were carried out at the Linac Coherent Light Source (LCLS) at the SLAC National Accelerator Laboratory. LCLS is an Office of Science User Facility operated for the U.S. Department of Science Office of Science by Stanford University under Contract No. DE-ACO2-76SF00515. LBNL part of the work is supported by the Director, Office of Science, of the U.S. Department of Energy under Contract No. DE-AC02-05CH1123.

REFERENCES

- [1] For example, E. L. Saldin, E. A. Schneidmiller, and M. V. Yurkov, Optics Communications 148 (1998) 383.
- [2] P. Heimann, O. Krupin, W. F. Schlotter, J. Turner, J. Krzywinski, F. Sorgenfrei, M. Messerschmidt, D. Bernstein, J. Chalupský, V. Hájková, S. Hau-Riege, M. Holmes, L. Juha, N. Kelez, J. Lüning, D.

- Nordlund, M. Fernandez Perea, A. Scherz, R. Soufli, W. Wurth, and M. Rowen, *Rev. Sci. Instrum.* 82, (2011) 093104.
- [3] D. Zhu, M. Cammarata, J. M. Feldkamp, D. M. Fritz, J. B. Hastings, S. Lee, H. T. Lemke, A. Robert, J. L. Turner, and Y. Feng, *Appl. Phys. Lett.* 101, (2012) 034103.
- [4] J. Feldhaus, E. L. Saldin, J. R. Schneider, E. A. Schneidmiller, M. V. Yurkov, *Optics Comm.* 140 (1997) 341.
- [5] Y. Feng, J. Hastings, P. Heimann, M. Rowen, J. Krzywinski, and J. Wu, "Optics for self-seeding soft x-ray FEL undulators", proceedings of 2010 FEL conference, Malmo, Sweden, (2010).
- [6] Y. Feng, "Compact Grating Monochromator Design for LCLSII Soft X-ray Self-Seeding", https://sites.google.com/a/lbl.gov/realizing_the_potential_of_seeded_fel_s_in_the_soft_x-ray_regime_workshop/talks
- [7] J. Amann, W. Berg, V. Blank, F.-J. Decker, Y. Ding, P. Emma, Y. Feng, J. Frisch, D. Fritz, J. Hastings, Z. Huang, J. Krzywinski, R. Lindberg, H. Loos, A. Lutman, H.-D. Nuhn, D. Ratner, J. Rzepiela, D. Shu, Yu. Shvyd'ko, S. Spampinati, S. Stoupin, S. Terentyev, E. Trakhtenberg, D. Walz, J. Welch, J. Wu, A. Zholents, and D. Zhu, *Nature Photonics* 180 (2012) 1038.
- [8] H. Peterson, *Optics Comm.* 40 (1982) 402.
- [9] J. Wu (unpublished).
- [10] B. Saleh and M. Teich, *Fundamentals of Photonics*. (New York: John Wiley & Sons, 1991), 26.
- [11] A. April and N. McCarthy, *Optics Comm.* 271(2007) 327.